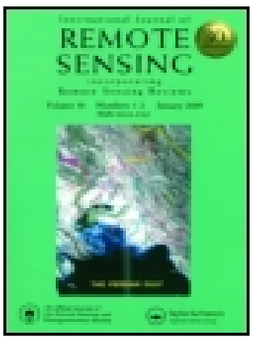

International Journal of Remote Sensing

ISSN: 0143-1161 (Print) 1366-5901 (Online) Journal homepage: https://www.tandfonline.com/loi/tres20

Potential of soil moisture retrieval for tropical peatlands in Indonesia using ALOS-2 L-band full-polarimetric SAR data

Y. Izumi, J. Widodo, H. Kausarian, S. Demirci, A. Takahashi, P. Razi, M. Nasucha, H. Yang & J. Tetuko S. S.

To cite this article: Y. Izumi, J. Widodo, H. Kausarian, S. Demirci, A. Takahashi, P. Razi, M. Nasucha, H. Yang & J. Tetuko S. S. (2019): Potential of soil moisture retrieval for tropical peatlands in Indonesia using ALOS-2 L-band full-polarimetric SAR data, International Journal of Remote Sensing, DOI: 10.1080/01431161.2019.1584927

To link to this article: https://doi.org/10.1080/01431161.2019.1584927

INTERNATIONAL JOURNAL OF REMOTE SENSING
https://doi.org/10.1080/01431161.2019.1584927

Taylor & Francis
Taylor & Francis Group

Potential of soil moisture retrieval for tropical peatlands in Indonesia using ALOS-2 L-band full-polarimetric SAR data

Y. Izumi [a], J. Widodo[b], H. Kausarian[c], S. Demirci[d], A. Takahashi[e], P. Razi [b], M. Nasucha[b], H. Yang[b] and J. Tetuko S. S. [b,e]

[a]Graduate School of Environmental Studies, Tohoku University, Sendai, Japan; [b]Graduate School of Advanced Integration Science, Chiba University, Chiba, Japan; [c]Engineering Geology Program, Faculty of Engineering, Universitas Islam Riau, Kota Pekanbaru, Indonesia; [d]Electrical and Electronic Faculty of Engineering, Mersin University, Mersin, Turkey; [e]Center for Environmental Remote Sensing (CEReS), Chiba University, Chiba, Japan

ABSTRACT

In this paper, a soil moisture retrieval from full-polarimetric synthetic aperture radar (SAR) data is investigated for sparsely vegetated soil surfaces. An improved retrieval method adapting the variations in vegetation is proposed by incorporating the generalized volume model into the polarimetric two-scale two-component model (PTSTCM). The feasibility of the method, termed as the adaptive PTSTCM, has been tested for tropical peatland sites in Indonesia which exhibit a variety of sparse vegetation cover on soil after land clearing activities. The *in situ* data were collected in March and August 2017 with the time domain reflectometry (TDR) probe for a total of 18 sample points over 11 regions. The method was applied to ALOS-2 L-band quad-pol SAR data that were acquired simultaneously with field measurements. We compared the results between the proposed adaptive PTSTCM and the original PTSTCM that utilizes specific types of volume model (i.e., randomly, horizontally, and vertically oriented volume models). Scatterplots of estimated versus measured *in situ* results reveal that the adaptive PTSTCM yields a root-mean-square error (RMSE) of 5.1vol.% and inversion rate of 35.0% and 58.5% for March and August data, respectively, which are found to be superior to those of the original PTSTCM.

ARTICLE HISTORY
Received 18 April 2018
Accepted 17 December 2018

1. Introduction

Tropical peatlands, being important carbon sinks and stores, play a critical role in carbon cycling between the earth surface and the atmosphere (Osaki et al. 2016). A total area of tropical peatlands on the Earth is 4441,025 km^2, which is spread out mostly in Southeast Asia, particularly in Indonesia and Malaysia. Indonesia alone has around 47% of the global tropical peatland area, where accumulated peat layers at the surface are mainly formed as extensive domes of a woody peat (Page, Rieley, and Banks 2011).

In Indonesia, especially in Kalimantan and Sumatra, a substantial amount of tropical peatlands has been deforested under the government's resettlement program in order

CONTACT Y. Izumi yutaizumi0927@gmail.com Graduate School of Environmental Studies, Tohoku University, Japan

to prepare agricultural areas for a plantation of oil palms, rubber, pulp trees, and food production (Osaki et al. 2016). A land transformation due to this program had increased the number of drainage canals required for conveying logged timbers and a land draining. In such cases, groundwater levels can get so low that capillary action cannot take place due to a spongy form of drained soil. As a result, the use of fire in conventional land clearing activities can give rise to a massive peat/forest fire. Once ignited, a spatially spreaded fire is difficult to be extinguished as they tend to flow downward and laterally with fast burn velocities (Usup et al. 2004). About 30.7% of peatlands in Indonesia are located in Sumatra island half of which takes place in Riau province (Gunawan et al. 2012). This region experiences a high annual peat/forest fire occurrence which produces an immense CO_2 emission thereby affecting the global climate. In addition, a transnational dense haze pollution resulted by a peat/forest fire is known for increasing aggregate adverse effects on humans' health and leading to traffic network damage. These fire-induced natural disasters often occur in the dry season of the year and may also be caused by a natural extreme weather phenomenon happened during the El Niño event.

Knowledge of a groundwater level is a key factor in knowing the hazard index of peat fire (Takahashi et al. 2004) and preventing ignition of deeper layers of peat soil which has difficulty to be extinguished (Usup et al. 2004). This information also contributes to a restoration confirmation of tropical peatlands as well as estimation of the CO_2 efflux and the carbon loss (Carlson, Goodman, and May-Tobin 2015; Hirano et al. 2014). Therefore, a continuous monitoring of fluctuations in groundwater levels is needed through regular measurements (Jaya et al. 2011; Ishii et al. 2016). Surface soil moisture can also alternatively be exploited in this task (Usup et al. 2004) because of its direct relationship with a groundwater level (Takahashi et al. 2004). In practice, a *in situ* field measurement technique is a cost-effective feasible solution to this problem, providing a long-term monitoring with a data logger. It can also be combined with a wireless network to extend its limited coverage to multitude field/regional scales. However, this technique is still not suitable for large-scale mapping applications, and thus its practicality and a coverage limitation should be compromised (Jagdhuber 2012; Sundari et al. 2012).

On the other hand, remote sensing techniques specifically synthetic aperture radar (SAR) has the potential to offer soil moisture information over wide areas in a single observation. SAR remote sensing is capable to provide high-resolution images even under cloudy conditions which are usually encountered in tropical areas. A sensitivity of SAR to soil moisture is based on the fact that backscattering intensity is mainly related to soil dielectric constant and surface roughness (Hajnsek, Pottier, and Cloude 2003), where the soil dielectric constant can be directly linked to the volumetric soil moisture by a well-known empirical polynomial equation (Topp, Davis, and Annan 1980). Since two or more unknown parameters are involved in the process, a multi-polarization measurement is necessary to retrieve the soil dielectric constant. To estimate volumetric soil moisture from polarimetric SAR data, several inversion approaches have been proposed for different soil and vegetation cover conditions and corresponding electromagnetic scattering models. These are mainly categorized into three types; empirical model (Zribi and Dechambre 2003), semi-empirical model (Oh 2004; Dubois, Van Zyl, and Engman 1995), and theoretical model (Fung and Chen 2010; Ulaby et al. 1982; Chen and Fung 1988). Formerly, inversion algorithms were mainly focused on bare soil surfaces due to

a lack of scattering models for surfaces with different scales of roughness. For example, the first-order small perturbation model (SPM) (Ulaby et al. 1982), being a widely used theoretical model, however, fails to describe cross-polarized and depolarized scatterings from random surfaces. To overcome these limitations, the X-Bragg model was proposed (Hajnsek, Pottier, and Cloude 2003) with an addition of a reflection symmetric depolarizing component to the first-order SPM. In this model, however, random orientations of scatterers are modelled with a uniformly distributed rotation angle of a local incidence plane which also limits an applicability of the model to different surface geometries. The recently proposed polarimetric two-scale model (PTSM) allows different distributions of the local incidence angle and the local incidence plane, and is shown to give more accurate results than those of the X-Bragg model (Iodice, Natale, and Riccio 2011, 2013).

Nevertheless, applying above methods for tropical peatland surfaces is expected to fail because of a widely spread vegetation cover over tropical regions. In applying surface scattering models to vegetated areas, a polarimetric decomposition concept presents a promising way which can be referred in the context of agricultural applications (Hajnsek et al. 2009; Jagdhuber et al. 2011; Huang, Wang, and Shang 2016; He et al. 2016; Ballester-Berman, Vicente-Guijalba, and Lopez-Sanchez 2013; Di; Martino et al. 2016). In particular, the polarimetric two-scale two-component model (PTSTCM) proposed by Martino *et al*. is only a method which combines the polarimetric decomposition concept with the PTSM, and revealed good agreement with *in situ* observations of volumetric soil moisture for agricultural areas (Di Martino et al. 2016). A two-component model-based decomposition method is employed in PTSTCM in which the surface scattering component is modelled by the PTSM, whereas the volume scattering component is chosen among three conventional volume types: random dipole orientation, vertical dipole orientation, and horizontal dipole orientation models (Yamaguchi et al. 2005). Although the PTSTCM provides a convenient way of modelling a variety of surface-vegetation cover scattering scenarios, this algorithm is not able to choose the proper volume model before obtaining retrieval results. In addition, since tropical peatlands exhibit a large variety of vegetation types, a more general description of the volume model is preferable. Among candidates, the parametric volume model such as the generalized volume model proposed by Arii *et al*. are seen to be very effective in representing a wide variety of vegetation types. Consequently, we herein propose a soil moisture retrieval scheme based on the PTSTCM which can iteratively find the appropriate volume scattering model within a variety of volume scattering models. To deal with a vegetation diversity in tropical peatlands, the volume scattering models are characterized by the generalized volume model.

In brief, we address to develop a soil moisture retrieval algorithm which is especially appropriate for tropical peatlands. The method was applied to ALOS-2 L-band full-polarimetric SAR data acquired over the Siak Regency, Riau province, Sumatra Island, Indonesia. We employed ALOS-2 data because L-band microwaves have a capability to penetrate vegetation and soil surfaces more than other mostly used bands of C-band and X-band. In order to validate our results, we collected *in situ* volumetric soil moisture at the same time as ALOS-2 observations. It is important to note that the PTSTCM is valid only on sparse vegetation fields because it assumes negligible double-bounce scattering components. Therefore, the investigated area was selected according to this constraint, which was decided to be open areas mainly after land clearing activities performed in

the past. Thus, the test sites were those scattered compound of sparse and slight vegetation which produce negligible double-bounce scattering. Although this is the main limitation of the proposed method, we hope that such an area is considered as the peat fire threatened area which is our focus.

The paper has the following organization. Section 2 describes the monitored study region, the ground-truth measurements, and the satellite overpass images at the same time of measurements. Section 3 introduces the proposed soil moisture retrieval method, whereas Section 4 shows derived moisture maps and their analyses with discussions. Finally, some conclusions are drawn in Section 5.

2. Field data

2.1. *Study region*

The study region was selected as the Siak Regency (100°10′59″ E, 0°20′49″ ∼ 1°16′30″ N) located within the Riau province of Indonesia. The region encompasses about 698,663 ha, around 75% of which consists of peatlands. In general, the Siak Regency has tropical climate with an average annual temperature and rainfall ranging from 25 to 32°C, and 1,359 to 4,078 mm y^{-1}, respectively. Topography is mainly flat with slope changing between 0° and 3° at height of 0 to 50 m above the sea level. The rainy season begins in October and ends in April, while the dry season begins in May and ends in September according to the government website (see the website at http://www.bmkg.go.id). A palm oil plantation is by far the main commodity in this region, and thus there are 20 palm oil refineries. Besides, agricultural areas such as rubber, coconut, sago, coffee, and cacao are also growing rapidly. Geological map of the entire prospect region is shown in Figure 1(a). There are mainly two types of geological formation; Young Superficial Deposits (Qp) and Older Superficial Deposits (Qh). Figure 1(a) depicts a spatial distribution and deposit contents of these formations. The Qp consists of clay, silts, clean gravels, vegetation raft, coral reefs, and peatland, whereas the Qh consists of clay, silts, clayey gravels, vegetation raft, and granite sands. Peatlands are distributed within the Qp segment indicated with green colour in Figure 1(a).

2.2. *SAR image data*

Full-polarimetric L-band (with 1.27 GHz centre frequency) ALOS-2 PALSAR-2 datasets were used to evaluate the usefulness of the proposed method. Acquisitions were performed on 25 March (scene 1) and 2 August 2017 (scene 2) with parameters shown in Table 1. Imaging swaths for each scene are depicted in Figure 1(b) with blue and red rectangles. Figure 1(b) shows a three-component model-based decomposition image of the segment outlined with black lines.

2.3. *Ground truth measurement*

Ground-truth data were acquired on approximate dates of the satellite data acquisition. Within the explored region, 11 open peatland zones were selected which were also confirmed based on Figure 1(a). A total of 18 test fields were then determined within

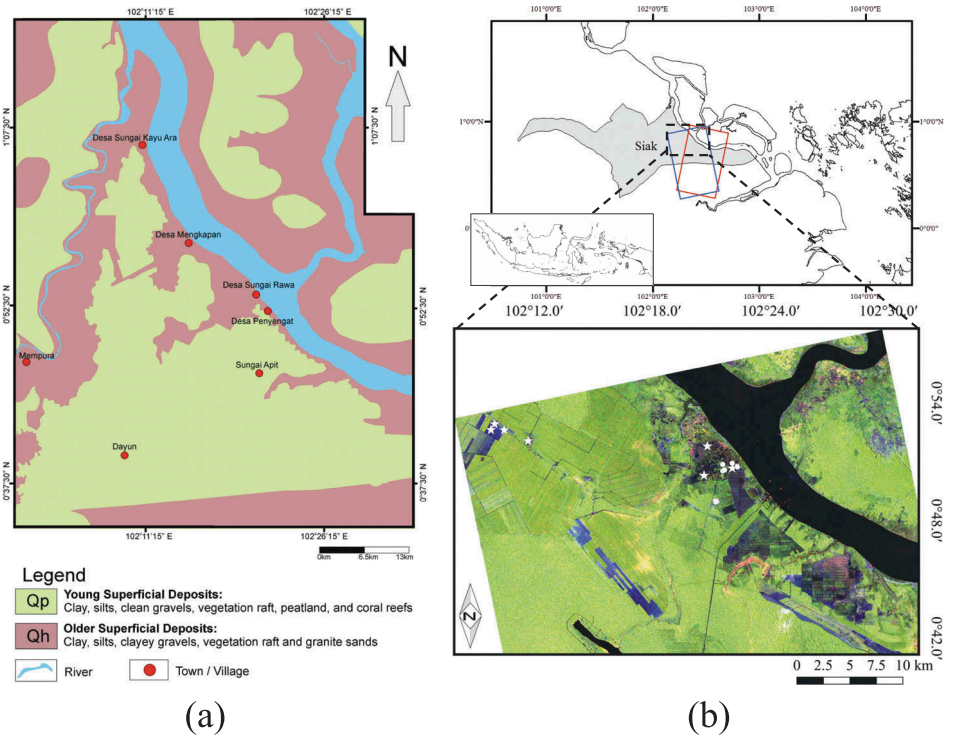

Figure 1. The study region in Indonesia. (a) A geological map showing a distribution of peatlands as green colour (b) Top: The location of the image swaths observed by ALOS-2 in March (blue) and August (red). Bottom: The three-component model-based decomposition image of the segment outlined with black lines and using blue for surface, red for double-bounce and green for volume scattering. The test fields are indicated with star (March) and circle (August) symbols, respectively.

Table 1. Summary of the full-polarimetric L-band ALOS-2 PALSAR-2 imaging data observed over the study region on 25 March (scene1) and 2 August (scene2). See Figure 1(b) for the corresponding image swaths.

Configuration	Scene1	Scene2
Acquisition date	25 March 2017	2 August 2017
Range resolution	6 m	6 m
Azimuth resolution	4.3 m	4.3 m
Incidence angle at image center	31.081°	31.081°
Orbit pass	Ascending	Descending

these zones which are labelled as shown in Table 2. M and A denote March and August data, respectively, and the lowercase letters indicate the fields within the subdivided zones. The habitat conditions of the fields are given in Table 2, showing the scientific name of dominant vegetation, vegetation height, and soil texture information that represents a rate of sand, silt, and clay. The type of peatland vegetation was not identified for some fields due to dried shrinkage condition, and therefore we blank them in Table 2. *In situ* volumetric soil moisture measurements were then made by means of the TDR probes (IMKO Trime Pico 32) for a depth of 11 cm from the surface. For each field, samples were collected at 12 randomly selected locations and averaged

Table 2. Soil and vegetation information of each measured field. M and A indicate field points of March and August, respectively.

Field #	Field condition	Species name	Vegetation height (cm)	Sand (%)	Silt (%)	Clay (%)
M1	Dried vegetation cover	–	–	53.48	39.46	7.06
M2	Sparse vegetation on rough surface	*Acasia mangium*	160	53.30	30.99	15.71
M3	Sparse vegetation	*Ptiridium caudatum*	90	67.00	24.63	8.37
M4	Sparse vegetation	*Ptiridium caudatum*	60	74.83	16.66	8.51
M5 a, b, c	Sparse vegetation	*Acasia mangium*	85	86.51	10.70	2.79
A1 a, b, c, d, e	Rough surface with a few logs after deforestation	–	–	76.67	17.32	6.01
A2	Burnt area covered by dried vegetation with burnt fallen tree branches and trunks	–	–	48.23	33.18	18.59
A3	Burnt area with burnt fallen tree branches and trunks	–	–	54.14	28.13	17.23
A4	Dried sparse vegetation	*Ptiridium caudatum*	65	71.36	21.36	7.28
A5	Burnt area with burnt fallen tree branches and trunks	–	–	47.37	34.96	17.67
A6 a, b	Sparse vegetation	*Imperata cylndrica*	75	70.19	19.61	10.20

Figure 2. Volumetric soil moisture measurement by the TDR probes.

to obtain a single estimated moisture value. Figure 2 shows our volumetric soil moisture measurements by the TDR probes at the tropical peatlands.

3. Soil moisture retrieval scheme with adaptive PTSTCM

We introduce a new soil moisture retrieval scheme based on the PTSTCM, which can adaptively find the appropriate volume scattering model, termed as adaptive PTSTCM. The adaptive PTSTCM assumes that scattering signals mostly come from ground and vegetation layers with the corresponding surface and volume scattering components, in which surface scattering is modelled by the PTSM whereas volume scattering is characterized by the Arii's generalized volume scattering model (Iodice, Natale, and Riccio 2011; Arii, van Zyl, and Kim 2010). Thus, it employs two-component model-based decomposition which proceeds in a similar manner as the PTSTCM. In the following, we first summarize the PTSM and the generalized volume model and then present the proposed moisture estimation scheme based on the adaptive PTSTCM.

3.1. *Surface scattering: PTSM*

In the original PTSM, rough surface scattering is modelled by assembling slightly rough facets that are subject to large-scale tilts. Figure 3 shows the geometry of a single facet rotated along local azimuth and range directions (Iodice, Natale, and Riccio 2011). The surface tilt results in variation of local incidence angles and local incidence planes around the line of sight. Two slope components, i.e., azimuth slope a and range slope b can be linked to both local incidence angle θ_l between the direction vector k and the normal vector of the tilted-facet n_{local} and the rotation angle of the incidence plane β with

$$\begin{aligned} \cos\theta_l &= \frac{\cos\theta_g + b\sin\theta_g}{\sqrt{1+a^2+b^2}}, \\ \tan\beta &= \frac{a}{-b\cos\theta_g + \sin\theta_g}, \end{aligned} \tag{1}$$

where θ_g is the global incidence angle between k and n_{local}.

Because two roughness scales are combined, i.e., slightly rough and very rough (caused by tilted facets), this surface model is a so-called two-scale model, where it would be reasonable to extend a validity range of a slightly rough presumption (Barrick and Peake 1968). This slight or 'small-scale' roughness can be statistically modelled as a zero-mean bandlimited fractional Brownian motion with the Hurst coefficient H_t and its height standard deviation s. While on the other hand, facets' random slopes a and b along range and azimuth directions, respectively, express 'large-scale' roughness (Di Martino et al. 2016; Iodice, Natale, and Riccio 2011). In case of the PTSM, a and b are expressed as independent zero-mean σ^2-variance Gaussian random variables. Each facet's size is assumed to be greater than wavelength and correlation length of the small-scale roughness, but much smaller than the sensor geometric resolution and the correlation length of the large-scale roughness.

In order to derive a covariance matrix model based on the PTSM, consider a rotated Bragg surface scattering given in Figure 3. Total scattered power from random tilted facets can be obtained by averaging a single covariance matrix over β and θ_l, or equivalently, slopes a and b together with their probability density functions (pdf) all having a zero-mean σ^2-variance Gaussian distribution. After Taylor series expansion of

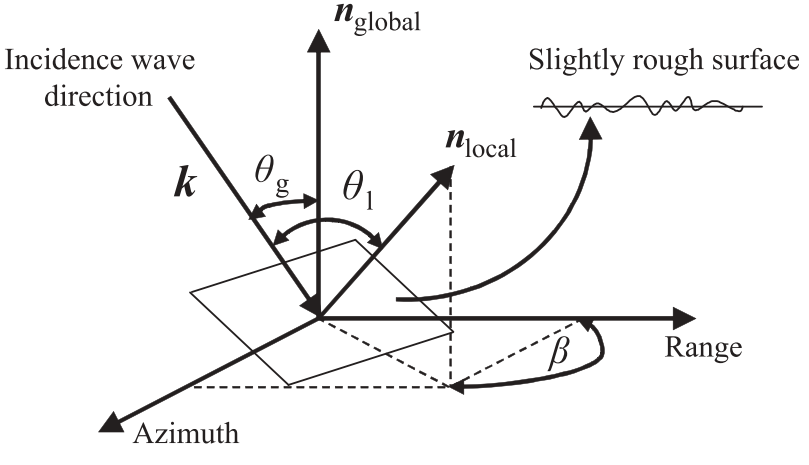

Figure 3. A geometry of a rotated single facet along both azimuth and range direction in the PTSM.

the closed form result around a= 0 and b= 0 and taking up to second order terms, covariance matrix elements of total scattered power are found at origin (Di Martino et al. 2016) as

$$\begin{bmatrix} \langle |S_{HH}|^2 \rangle & \sqrt{2}\langle S_{HH}S_{HV}^* \rangle & \langle S_{HH}S_{VV}^* \rangle \\ \sqrt{2}\langle S_{HV}S_{HH}^* \rangle & 2\langle |S_{HV}|^2 \rangle & \sqrt{2}\langle S_{HV}S_{VV}^* \rangle \\ \langle S_{VV}S_{HH}^* \rangle & \sqrt{2}\langle S_{VV}S_{HV}^* \rangle & \langle |S_{VV}|^2 \rangle \end{bmatrix}$$

$$\simeq s^2 f_s(\varepsilon,\ H_t) \begin{bmatrix} |\beta_r(\varepsilon)|^2(1+\delta_H(\varepsilon)\sigma^2) & 0 & \beta_r(\varepsilon)(1+\delta_{HV}(\varepsilon)\sigma^2) \\ 0 & 2\delta_X(\varepsilon)\sigma^2 & 0 \\ C_{13}^* & 0 & (1-\delta_V(\varepsilon)\sigma^2) \end{bmatrix}, \tag{2}$$

where

$$\begin{aligned}
f_s(\varepsilon,\ H_t) &= k^4 \cos^4\theta \left|R_v(\theta_g,\varepsilon)\right|^2 W_n(\theta_g,H_t),\\
R_h(\theta_g,\varepsilon) &= \frac{\cos\theta_g - \sqrt{\varepsilon-\sin^2\theta_g}}{\cos\theta_g + \sqrt{\varepsilon-\sin^2\theta_g}},\\
R_v(\theta_g,\varepsilon) &= \frac{\varepsilon\cos\theta_g - \sqrt{\varepsilon-\sin^2\theta_g}}{\varepsilon\cos\theta_g + \sqrt{\varepsilon-\sin^2\theta_g}},\\
\beta_r(\varepsilon) &= \frac{R_h(\theta_g,\varepsilon)}{R_v(\theta_g,\varepsilon)},\\
\delta_X(\varepsilon) &= \frac{|1-\beta_r(\varepsilon)|^2}{\sin^2(\theta_g)},\\
\delta_V(\varepsilon) &= 2\,\mathrm{Re}\left\{\frac{1-\beta_r(\varepsilon)}{\sin^2(\theta_g)}\right\} - \frac{C_2^{VV}(\varepsilon,H_t)}{f_s(\varepsilon,H_t)},\\
\delta_H(\varepsilon) &= 2\,\mathrm{Re}\left\{\frac{1-\beta_r(\varepsilon)}{\beta_r(\varepsilon)\sin^2(\theta_g)}\right\} - \frac{C_2^{HH}(\varepsilon,H_t)}{|\beta_r(\varepsilon)|^2 f_s(\varepsilon,H_t)},\\
\delta_{HV}(\varepsilon) &= \frac{1-\beta_r(\varepsilon)}{\beta_r(\varepsilon)\sin^2(\theta_g)} - \frac{1-\beta_r^*(\varepsilon)}{\sin^2(\theta_g)} + \frac{C_2^{HV}(\varepsilon,H_t)}{\beta_r(\varepsilon) f_s(\varepsilon,H_t)},\\
C_2^{pq}(\varepsilon,\ H_t) &= \frac{1}{2}\frac{\partial^2\left(W_n(\theta_g,H_t)k^4\cos^4\theta_l R_p(\theta_g,\varepsilon)R_q^*(\theta_g,\varepsilon)\right)}{\partial a^2}\bigg|_{a=b=0}\\
&\quad + \frac{1}{2}\frac{\partial^2\left(W_n(\theta_g,H_t)k^4\cos^4\theta_l R_p(\theta_g,\varepsilon)R_q^*(\theta_g,\varepsilon)\right)}{\partial b^2}\bigg|_{a=b=0},
\end{aligned}$$

where k is a wavenumber, $W_n(\theta_g,H_t)$ is a normalized power spectral density of small-scale roughness (see (Iodice, Natale, and Riccio 2011)), ε is a complex dielectric constant, and p and q denote the receive and transmit polarization, respectively. It is worth noting that $\beta_r(\varepsilon)$ and $\delta_X(\varepsilon)$ are independent parameters of the Hurst coefficients H_t whereas $\delta_H(\varepsilon)$, $\delta_V(\varepsilon)$, and $\delta_{HV}(\varepsilon)$ are functions that weakly depend on H_t. Therefore, the PTSM preliminarily fixes H_t, which we take as 0.5 in this study. We also treated the ε as a real positive function since an effect of its imaginary part is insignificant within a frequency range of our satellite data.

3.2. *Volume scattering: generalized volume scattering model*

In SAR polarimetry, volume scattering from vegetation canopies has generally been modelled as a cloud of dipole-like scattering. A statistical formulation of volume scattering can be achieved by an angular averaging of the covariance/coherency matrix of a dipole oriented by an angle θ together with a pdf of the corresponding angular distribution (Freeman and Durden 1998; Yamaguchi et al. 2005). The pdf $p(\theta)$ of

randomly, horizontally, and vertically oriented dipoles are $p(\theta) = (1/2\pi)$, $p(\theta) = (1/2)\sin\theta$, and $p(\theta) = (1/2)\cos\theta$, respectively, whereas the corresponding covariance matrices are

$$\begin{aligned}
&\tfrac{1}{8}\begin{bmatrix}3&0&1\\0&2&0\\1&0&3\end{bmatrix} \quad \text{randomly oriented volume},\\
&\tfrac{1}{15}\begin{bmatrix}8&0&2\\0&4&0\\2&0&3\end{bmatrix} \quad \text{horizontally oriented volume},\\
&\tfrac{1}{15}\begin{bmatrix}3&0&2\\0&4&0\\2&0&8\end{bmatrix} \quad \text{vertically oriented volume}.
\end{aligned} \tag{3}$$

Although these three volume scattering components have been widely exploited in conventional model-based decomposition techniques, their validity for several types of vegetation may deteriorate significantly. To overcome this limitation, Arii *et al*. proposed the *n*th power cosine-squared pdf as a generalized angular distribution function (Arii, van Zyl, and Kim 2010)

$$p_{\text{general}}(\theta,\,\theta_0,\,n) = \frac{\left|\{\cos^2(\theta-\theta_0)\}^n\right|}{\displaystyle\int_0^{2\pi}\left|\{\cos^2(\theta-\theta_0)\}^n\right|d\theta}, \tag{4}$$

where θ_0 is a mean orientation angle related to the canopy orientation, and n indicates a degree of randomness related to the scattering entropy, with the randomness decreases as the n increases (Arii, van Zyl, and Kim 2010). Upon adopting this pdf in the angular averaging process of the dipole's covariance matrix $[\mathbf{C}_{\text{dipole}}]$, we can obtain the parameterized volume scattering model as

$$\begin{aligned}
\left\langle\left[\mathbf{C}_{\text{vol}}^{\text{general}}\right](\theta_0,n)\right\rangle &= \frac{1}{\displaystyle\int_0^{2\pi}\cos^{2n}(\theta-\theta_0)d\theta}\int_0^{2\pi}\left[\mathbf{C}_{\text{dipole}}\right]\cos^{2n}(\theta-\theta_0)d\theta\\
&= [\mathbf{C}_a] + \frac{2n}{n+1}[\mathbf{C}_\beta(2\theta_0)] + \frac{n(n-1)}{(n+1)(n+2)}[\mathbf{C}_\gamma(4\theta_0)],
\end{aligned} \tag{5}$$

where

$$\begin{aligned}
[\mathbf{C}_a] &= \tfrac{1}{8}\begin{bmatrix}3&0&1\\0&2&0\\1&0&3\end{bmatrix},\\
[\mathbf{C}_\beta(2\theta_0)] &= \tfrac{1}{8}\begin{bmatrix}-2\cos 2\theta_0 & \sqrt{2}\sin 2\theta_0 & 0\\ \sqrt{2}\sin 2\theta_0 & 0 & \sqrt{2}\sin 2\theta_0\\ 0 & \sqrt{2}\sin 2\theta_0 & 2\cos 2\theta_0\end{bmatrix},\\
[\mathbf{C}_\gamma(4\theta_0)] &= \tfrac{1}{8}\begin{bmatrix}\cos 4\theta_0 & -\sqrt{2}\sin 4\theta_0 & -\cos 4\theta_0\\ -\sqrt{2}\sin 4\theta_0 & -2\cos 4\theta_0 & \sqrt{2}\sin 4\theta_0\\ -\cos 4\theta_0 & \sqrt{2}\sin 4\theta_0 & \cos 4\theta_0\end{bmatrix}.
\end{aligned}$$

The models in (3) can also be represented with this model through proper values of (n, θ_0); that is (n= 0), (n= 0.5, θ_0= 0) and (n= 0.5, θ_0=π/2) corresponds to randomly, horizontally and vertically distributed dipoles, respectively. It is also worth noting that (5) is no longer reflection symmetric, except for two specific mean orientation angles (e.g., θ_0= 0 and π/2).

3.3. *Adaptive PTSTCM*

In our approach, the measured covariance matrix $[\mathbf{C}_{\text{measured}}]$ is modelled as a linear sum of two pre-defined physical scattering models, i.e., the PTSM and the generalized volume scattering model:

$$\begin{aligned}[\mathbf{C}_{\text{measured}}] &= s^2 f_s [\mathbf{C}_{\text{surface}}] + f_v \left[\mathbf{C}_{\text{vol}}^{\text{general}}(\theta_0,\ n)\right] \\ &= s^2 f_s(\varepsilon,\ H_t) \begin{bmatrix} |\beta_r(\varepsilon)|^2(1+\delta_H(\varepsilon)\sigma^2) & 0 & \beta_r(\varepsilon)(1+\delta_{HV}(\varepsilon)\sigma^2) \\ 0 & 2\delta_X(\varepsilon)\sigma^2 & 0 \\ C_{13}^* & 0 & (1-\delta_V(\varepsilon)\sigma^2) \end{bmatrix} \\ &\quad + f_v \begin{bmatrix} V_{11}(\theta_0,\ n) & 0 & V_{13}(\theta_0,\ n) \\ 0 & 2V_{13}(\theta_0,\ n) & 0 \\ V_{13}^*(\theta_0,\ n) & 0 & V_{33}(\theta_0,\ n) \end{bmatrix},\end{aligned} \tag{6}$$

where f_v denotes volume scattering power.

In a recent study, Martino *et al*. used two observables to retrieve volumetric soil moisture under moderate vegetation conditions, which are named as 'modified Co-polarized ratio' and 'modified Correlation coefficient' as

$$\begin{aligned}\text{Copol} &= \frac{\left\langle |S_{HH}|^2 \right\rangle - \frac{V_{11}(\theta_0,\, n)}{V_{13}(\theta_0,\, n)} \left\langle |S_{HV}|^2 \right\rangle}{\left\langle |S_{VV}|^2 \right\rangle - \frac{V_{33}(\theta_0,\, n)}{V_{13}(\theta_0,\, n)} \left\langle |S_{HV}|^2 \right\rangle}, \\ \text{Corr} &= \frac{\left| \left\langle S_{HH} S_{VV}^* \right\rangle - \left\langle |S_{HV}|^2 \right\rangle \right|}{\sqrt{\left(\left\langle |S_{HH}|^2 \right\rangle - \frac{V_{11}(\theta_0,\, n)}{V_{13}(\theta_0,\, n)} \left\langle |S_{HV}|^2 \right\rangle \right) \left(\left\langle |S_{VV}|^2 \right\rangle - \frac{V_{33}(\theta_0,\, n)}{V_{13}(\theta_0,\, n)} \left\langle |S_{HV}|^2 \right\rangle \right)}}.\end{aligned} \tag{7}$$

These observables depend only on the root-mean-square (RMS) slope of the large-scale roughness σ and the relative dielectric constant ε, because the small-scale roughness and f_v are cancelled out (Di Martino et al. 2016). Note also that the original PTSTCM fixes the volume scattering covariance matrix by choosing from three conventional models given in Equation (3). Therefore, it is possible to retrieve ε and σ by comparing the measured Copol and Corr with their theoretical values. However, since volume components are still unknown in case of the generalized volume scattering model, the retrieved ε and σhave now become dependent on the values of θ_0 and n. To find an appropriate pair of ε and σ within $\varepsilon(\theta_0,n)$ and $\varepsilon(\sigma,n)$, two unknown parameters θ_0 and n are optimally selected in our algorithm as explained in the following.

Our approach is based on the idea that the volume scattering model that fits in best with the measured data must preserve the physically based modelling of Equation (6) holding the fundamental law of energy conservation. As pointed out by Van Zyl *et al*., the model-based decomposition suffers negative powers from individual terms which obviously breaks this law (van Zyl, Arii, and Kim 2011). Nevertheless, the criterion that minimizes the residual covariance matrix $[\mathbf{C}_{\text{residual}}(\theta_0, n)]$ can be adopted to find the optimal volume scattering model by varying θ_0 and n, where $[\mathbf{C}_{\text{residual}}(\theta_0, n)]$ is the residual after subtraction of surface and volume terms from the measured covariance matrix, expressed as

$$\begin{aligned}[\mathbf{C}_{\text{residual}}(\theta_0, n)] &= [\mathbf{C}_{\text{measured}}] - s^2 f_s(\theta_0, n)[\mathbf{C}_{\text{surface}}(\theta_0, n)] \\ &\quad - f_v(\theta_0, n)\left[\mathbf{C}_{\text{vol}}^{\text{general}}(\theta_0, n)\right].\end{aligned} \tag{8}$$

To calculate $[\mathbf{C}_{\text{residual}}(\theta_0, n)]$, it is required to determine the rest of the unknown parameters $[\mathbf{C}_{\text{surface}}(\theta_0, n)]$, $s^2 f_s(\theta_0, n)$ and $f_v(\theta_0, n)$. These quantities can be obtained by solving (6) after determining corresponding ε and σ by the original PTSTCM (expressions are reported in (Di Martino et al. 2016)). After getting all possibilities of $[\mathbf{C}_{\text{residual}}(\theta_0, n)]$, we straightforwardly evaluate the total power TP of $[\mathbf{C}_{\text{residual}}(\theta_0, n)]$ by summing the eigenvalues λ_i of $[\mathbf{C}_{\text{residual}}(\theta_0, n)]$

$$\text{TP} = \lambda_1 + \lambda_2 + \lambda_3. \tag{9}$$

We then choose the best-fit θ_0 and n pair that minimizes TP. It should be noted that θ_0 is assumed as either 0 or $\pi/2$ since both measured and volume covariance matrices will have a reflection symmetry for most natural surfaces. As for n, a value within the range 0–10 is taken with a step size of 0.5 in this paper.

Furthermore, to avoid unreliable retrieved results, we restricted volume scattering intensity $f_v(\theta_0, n)$ using mathematically derived maximum $f_v(\theta_0, n)$ ($f_v^{\max}(\theta_0, n)$) calculated by the non-negative eigenvalue method (van Zyl, Arii, and Kim 2011), and the pixels whose $f_v(\theta_0, n)$ higher than $f_v^{\max}(\theta_0, n)$ are not inverted. Also, the pixels which suffer $s^2 f_s(\theta_0, n)<0$, $\varepsilon(\theta_0,n)<2.5$, $\varepsilon(\theta_0,n)>40$, and $\sigma(\theta_0,n)>0.4$ are eliminated within the algorithm to obtain only physically meaningful results.

The retrieved ε is further processed to estimate volumetric soil moisture (m_v) through the widely used empirical polynomial equation of Topp *et al*. (Topp, Davis, and Annan 1980). This equation is employed because it depends only on the real part of the relative dielectric constant, as

$$m_v = -5.3 \cdot 10^{-2} + 2.92 \cdot 10^{-2}\varepsilon - 5.5 \cdot 10^{-4}\varepsilon^2 + 4.3 \cdot 10^{-6}\varepsilon^3. \tag{10}$$

The steps of the adaptive PTSTCM algorithm is described in Figure 4, and can be summarized as followings:

- A wide variety of vegetation can be considered by employing the generalized volume scattering model.
- A criterion that minimizes $[\mathbf{C}_{\text{residual}}(\theta_0, n)]$ is employed to select the best-fit volume scattering model.
- Only physically meaningful results are obtained by several constrained conditions.

4. Results and discussion

Prior to an application of the proposed method, the image datasets were preprocessed through several steps. Firstly, the refined Lee filter with a 5×5 window was applied to reduce speckle. Among the possibilities, this speckle filtering was selected since it preserves polarimetric information in homogeneous areas and maintains image sharpness (Lee, Grunes, and De Grandi 1999). The speckle filtered polarimetric SAR data were further processed through the geocoding.

Afterwards, because our model assumed negligible double-bounce and dense vegetation scattering, pixels with these features were eliminated. For double-bounce scattering, a signum of $Imag(S_{HH}S_{VV}^*)$ criterion was adopted (Jagdhuber 2012), so that pixels satisfying the following condition:

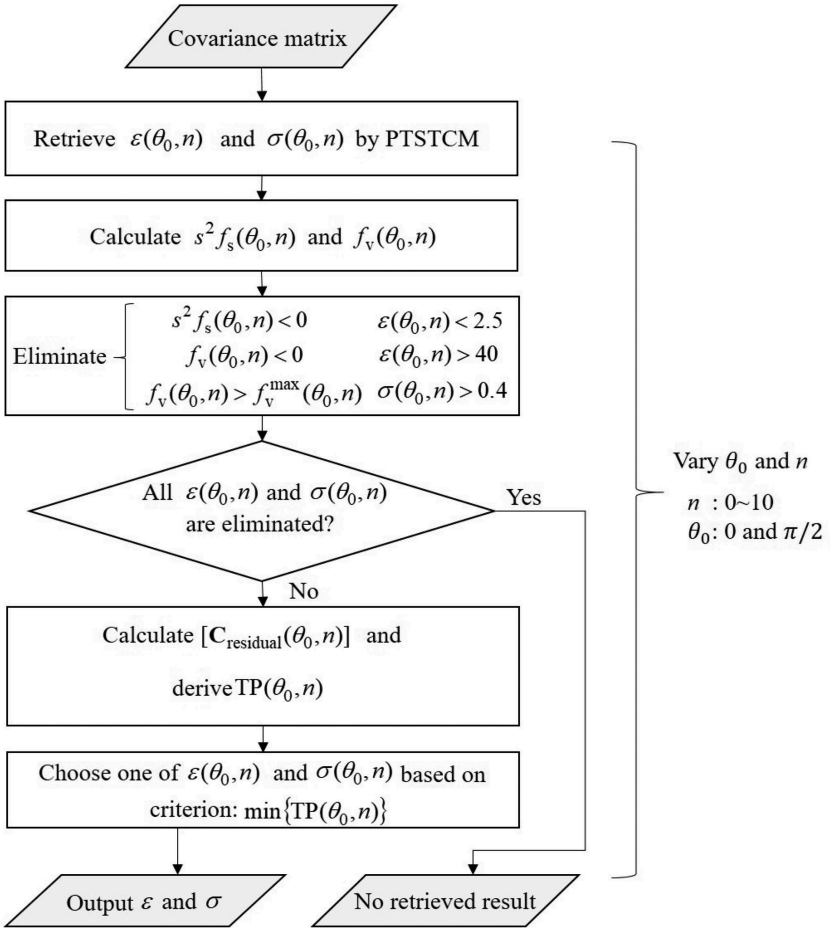

Figure 4. The adaptive PTSTCM algorithm.

$$\mathrm{Imag}(S_{HH}S_{VV}^*) < 0, \tag{11}$$

were eliminated. In fact, a signum of $\mathrm{Real}(S_{HH}S_{VV}^*)$ criterion seems also a possible way to separate surface and double-bounce scattering (Freeman and Durden 1998). However, the recent study (Jagdhuber 2012) validated the applicability of the $\mathrm{Imag}(S_{HH}S_{VV}^*)$ criterion for agricultural areas, where $\mathrm{Real}(S_{HH}S_{VV}^*)$ revealed inconsistency with actual field conditions. For dense vegetation or forested area scattering, pixels that meet

$$10\log_{10}\frac{\langle|S_{HV}|^2\rangle}{\langle|S_{VV}|^2\rangle} > -8.2391\ [\mathrm{dB}], \tag{12}$$

were discarded. This cross-polarized ratio criterion is based on the fact that Martino *et al.* showed pixels whose cross-polarized ratio greater than −8.2391 dB (0.15) are no longer valid for the PTSTCM processing. We applied these two criteria to geocoded SAR images, followed by retrieving volumetric soil moisture. Resulted soil moisture images were also averaged approximately by 10 × 10 pixels in each measured point.

4.1. *Results*

The volumetric soil moisture maps retrieved by the proposed adaptive PTSTCM for March and August data are shown in Figure 5(a,b) respectively, together with the photographs of each examined field. These maps were obtained through the Inverse Distance Weighted (IDW) interpolation method for continuous data, where we also masked the river section and areas which show poor density of inversion pixels, in addition to pixels satisfying Equation (11) and (12).

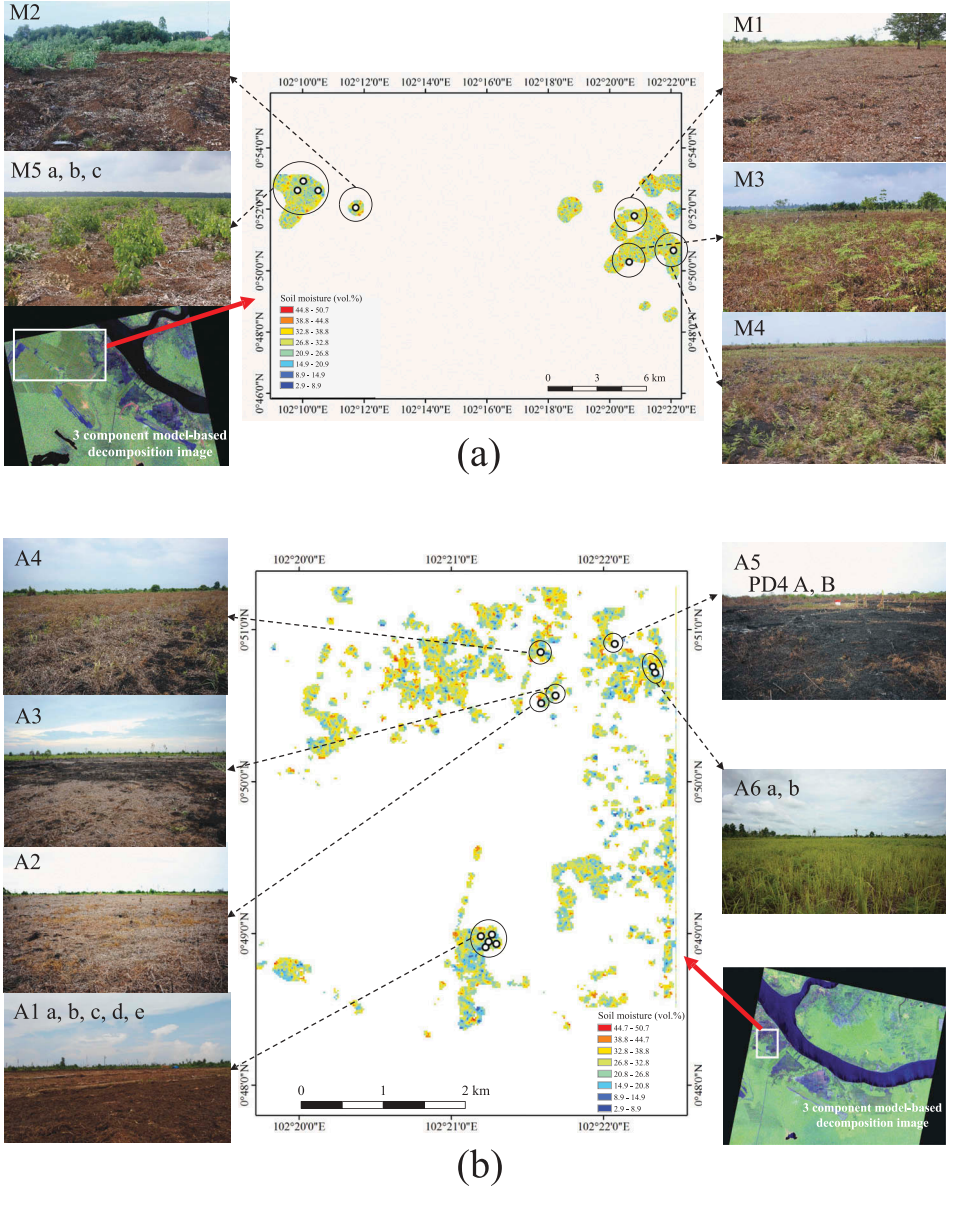

Figure 5. Soil moisture maps produced by the adaptive PTSTCM with photographs of each field. The location of map is indicated using a white rectangular box on the three component model-based decomposition SAR image. (a) Result produced by SAR data on 25 March. (b) Result produced by SAR data on 2 August.

To validate the feasibility of the adaptive PTSTCM, its results are compared with the original PTSTCM employing conventional three types of volume model (in (3)). The scatter plots of the estimated versus ground-truth data for the adaptive PTSTCM, the PTSTCM with randomly oriented volume, the PTSTCM with horizontally oriented volume, and the PTSTCM with vertically oriented volume are presented in Figure 6. For Figure 6(b,c,d), some field point results are not displayed because there is no inverted pixel at these field points. As a quantitative analysis, RMS error (RMSE) is derived for all results. The adaptive PTSTCM result yields RMSE of 5.1 vol.%, while the PTSTCM with randomly, horizontally, vertically oriented volume shows 10.1, 10.1, and 10.5 vol.%, respectively. These values clearly indicate that the adaptive PTSTCM gives better retrieval results than the other methods in terms of RMSE. Furthermore, we calculated the inversion rate which specifies an amount of successfully inverted pixels relative to the total pixels of the SAR image

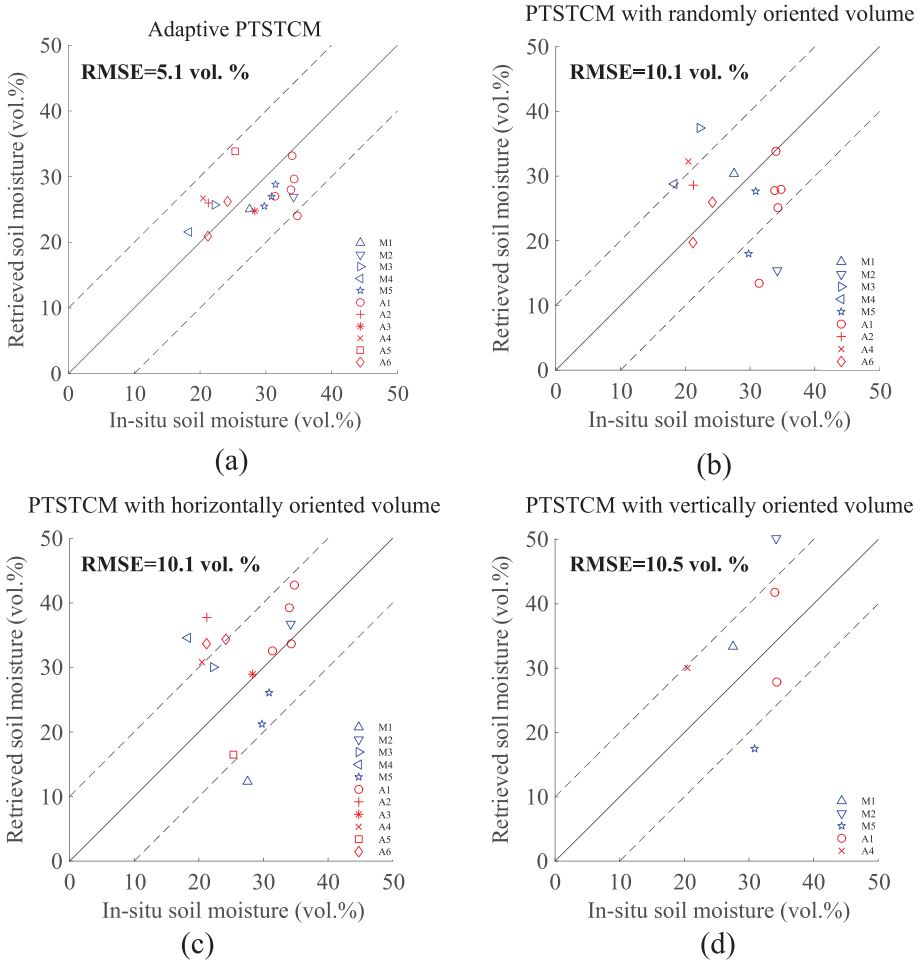

Figure 6. Scatter plots of retrieved soil moisture results versus *in situ* soil moisture results at 0–11 cm depth. The blue symbols show data on 25 March, whereas the red symbols show data on 2 August. (a) The adaptive PTSTCM; (b) The PTSTCM with randomly oriented volume; (c) The PTSTCM with horizontally oriented volume; (d) The PTSTCM with vertically oriented volume.

Table 3. Inversion rates for both acquisition dates of the adaptive PTSTCM and the PTSTCM with volume models of (2).

Date	Adaptive volume (%)	PTSTCM with randomly oriented volume (%)	PTSTCM with horizontally oriented volume (%)	PTSTCM with vertically oriented volume (%)
25 March 2017	35.0	9.5	7.1	0.3
2 August 2017	58.5	8.8	7.4	0.9

masked by $\mathrm{Imag}(S_{HH}S_{VV}^{*})$ and the cross-polarized ratio criteria. In Table 3, inversion rates of the four methods are tabulated for the two datasets. In each case, the adaptive PTSTCM offers the highest inversion rates with 35.0% for March data and 58.5% for August data.

4.2. *Discussion*

There are no known reports of the SAR-based soil moisture retrieval applied to tropical peat soils. These soils include a wide variety of live vegetation and residual vegetation (dead vegetation in post-fire soils) which makes modelling of their backscatter data difficult and uncertain. This, in turn, may impart a significant degradation in moisture mapping performance. Nevertheless, our adaptive model shows a reasonable accuracy of RMSE and inversion rate over final volumetric soil moisture maps, demonstrating its applicability for these challenging land covers.

Despite, the proposed adaptive model, as well as the original PTSTCM, both assume soil types which exhibit little double-bounce scattering. To examine the validity of this assumption for the investigated areas, consider some of the selected fields A1, A2, A3, and A5 which hold several burnt branches and fallen tree trunks, as specified in Table 2. Branches are expected to produce dominant volume scattering mechanisms since they behave as a cloud of randomly distributed dipoles. This can be confirmed by relevant results of A1, A2, A3, and A5 in Figure 6 since they yield different estimated values depending on the type of the volume model used. On the other hand, objects that are large in the wavelength scale, such as burnt tree trunks, are expected to show dominant double-bounce scattering events, which are not handled by the retrieval algorithm. This phenomenon can also be confirmed by means of identification of non-inverted pixels as burnt tree trunks. This issue will be considered in future extended work.

Noting that scattering mechanisms from different surfaces may vary markedly with the incidence angle and the wavelength, a performance of the method can be enhanced via investigating and selecting the optimal ranges of these parameters. According to the literature (Iodice, Natale, and Riccio 2011; Di; Martino et al. 2016), the PTSM as well as the PTSTCM indicate insensitivity to soil moisture variation of Copol and Corr in Equation (7) with steeper incidence angles. It is inferred that shallower incidence angles are more sensitive to underlying soil conditions, giving better RMSE and inversion rate values, and thus more suitable for moisture mapping.

It is also noting about a selection of a centre frequency for the tropical peatland monitoring. It is well known that a centre frequency affects penetration depth, where penetration depth increases as a centre frequency lower (Kausarian et al. 2017). Because our target fields contain vegetation, it is preferable to use lower frequencies so that the vegetation effect can be minimized as much as possible. Lower frequencies are also capable of retrieving the deeper subsurface soil moisture of the peatland which may help prevention

of ignition of the deep peat fire (see Section 1) more accurately than the surface soil moisture monitoring. As an alternative to L-band which is our selected frequency band in this paper, the future European Space Agency (ESA) BIOMASS mission of P-band (centre frequency 435 MHz) earth observation satellite can be cited (Arcioni et al. 2014). With this observation, it will be possible to monitor the peatland subsurface from 0.4 m to 2 m, by neglecting sparse vegetation and increasing a valid range of the surface roughness. Correspondingly, the ground truth measurement method is also differentiated. For example, employing low-frequency ground penetrating radar (GPR) allows the straightforward *in situ* measurement of the vertical soil moisture profile up to deeper subsurface which is previously conducted by the soil moisture retrieval study (Koyama et al. 2017).

5. Conclusion

In this paper, we demonstrated a novel method for retrieving volumetric soil moisture maps using full-polarimetric SAR data for tropical peatland areas. Termed as the adaptive PTSTCM, the method is especially appropriate for sparsely vegetated soil surfaces and is based on incorporation of the generalized volume model into the original PTSTCM. An applicability and an accuracy of the method have been assessed in tropical peatland fields of Indonesia using L-band ALOS-2 SAR data. Compared to the original PTSTCM which employs conventional three volume models (randomly, horizontally, and vertically oriented), our method selects the proper volume model in an adaptive manner and thus showed higher accuracies of up to 5.0793vol.% of RMSE and 58.5294% of inversion rate for our study sites. With this analysis, the feasibility of the adaptive PTSTCM was confirmed specifically for open areas with a variety of sparse vegetation. The method has the following features;

- It is capable to adaptively find the appropriate volume scattering model by incorporating the generalized volume model to compensate the vegetation effect in the soil moisture retrieval.
- It is constructed based on the PTSTCM, and thus it can be valid only on sparsely vegetated fields.
- Within the method, only physically meaningful results are inverted by the several constraint conditions.

With a further investigation of the different incidence angles and frequencies, this method could produce more precise and effective retrieval results as discussed in Section 4. In addition, a time-series observation should be conducted to deal with more variation of field conditions, weather conditions, and seasons, needed for a practical social implementation to investigate a deeper understanding of a relationship between peat fire mechanism and soil moisture.

Acknowledgments

We gratefully acknowledge financial which supported by the fourth Japan Aerospace Exploration Agency (JAXA) ALOS Research Announcement under Grant 1024, by the sixth JAXA ALOS Research Announcement under Grant 3170, by the Japanese Government National Budget (Special Budget for

Project) FY 2015 under Grant 2101, by Grand-in-Aid for JSPS Research Fellows 18J20104. We also would like to thank Universitas Islam Riau as the research collaboration partner as well as the international partner and Regency of Siak as the partner who provides the field during the research.

Disclosure statement

No potential conflict of interest was reported by the authors.

Funding

This work was supported by the Japan Aerospace Exploration Agency [1024,3170];Japan Society for the Promotion of Science [18J20104];Japanese Government National Budget [2101].

ORCID

Y. Izumi http://orcid.org/0000-0001-6554-3880
P. Razi http://orcid.org/0000-0001-5347-0055
J. Tetuko S. S. http://orcid.org/0000-0002-4036-6854

References

Arcioni, M., P. Bensi, M. Fehringer, F. Fois, C.-C. L. Florence H´Elière, and K. Scipal. 2014. "The Biomass Mission, Status of the Satellite System." In *Geoscience and Remote Sensing Symposium (IGARSS), 2014 IEEE International*, 1413–1416. Quebec City, Canada: IEEE.

Arii, M., J. J. van Zyl, and Y. Kim. 2010. "A General Characterization for Polarimetric Scattering from Vegetation Canopies." *IEEE Transactions on Geoscience and Remote Sensing* 48 (9): 3349–3357. doi:10.1109/TGRS.2010.2046331.

Ballester-Berman, J. D., F. Vicente-Guijalba, and J. M. Lopez-Sanchez. 2013. "Polarimetric SAR Model for Soil Moisture Estimation over Vineyards at C-Band." *Progress In Electromagnetics Research* 142: 639–665. doi:10.2528/PIER13071702.

Barrick, D. E., and W. H. Peake. 1968. "A Review of Scattering from Surfaces with Different Roughness Scales." *Radio Science* 3 (8): 865–868. doi:10.1002/rds196838865.

Carlson, K. M., L. K. Goodman, and C. C. May-Tobin. 2015. "Modeling Relationships between Water Table Depth and Peat Soil Carbon Loss in Southeast Asian Plantations." *Environmental Research Letters* 10 (7): 074006. doi:10.1088/1748-9326/10/7/074006.

Chen, M. F., and A. K. Fung. 1988. "A Numerical Study of the Regions of Validity of the Kirchhoff and Small-Perturbation Rough Surface Scattering Models." *Radio Science* 23 (2): 163–170. doi:10.1029/RS023i002p00163.

Dubois, P. C., J. Van Zyl, and T. Engman. 1995. "Measuring Soil Moisture with Imaging Radars." *IEEE Transactions on Geoscience and Remote Sensing* 33 (4): 915–926. doi:10.1109/36.406677.

Freeman, A., and S. L. Durden. 1998. "A Three-Component Scattering Model for Polarimetric SAR Data." *IEEE Transactions on Geoscience and Remote Sensing* 36 (3): 963–973. doi:10.1109/36.673687.

Fung, A. K., and K.-S. Chen. 2010. *Microwave Scattering and Emission Models for Users*. Boston: Artech house.

Gunawan, H., S. Kobayashi, K. Mizuno, and Y. Kono. 2012. "Peat Swamp Forest Types and Their Regeneration in Giam Siak Kecil-Bukit Batu Biosphere Reserve, Riau, East Sumatra, Indonesia." *Mires & Peat*, Vol. 10, 1–17.

Hajnsek, I., E. Pottier, and S. R. Cloude. 2003. "Inversion of Surface Parameters from Polarimetric SAR." *IEEE Transactions on Geoscience and Remote Sensing* 41 (4): 727–744. doi:10.1109/TGRS.2003.810702.

Hajnsek, I., T. Jagdhuber, H. Schon, and K. P. Papathanassiou. 2009. "Potential of Estimating Soil Moisture under Vegetation Cover by Means of Pol- SAR." *IEEE Transactions on Geoscience and Remote Sensing* 47 (2): 442–454. doi:10.1109/TGRS.2008.2009642.

He, L., R. Panciera, M. A. Tanase, J. P. Walker, and Q. Qin. 2016. "Soil Moisture Retrieval in Agricultural Fields Using Adaptive Model-Based Polarimetric Decomposition of SAR Data." *IEEE Transactions on Geoscience and Remote Sensing* 54 (8): 4445–4460. doi:10.1109/TGRS.2016.2542214.

Hirano, T., K. Kusin, S. Limin, and M. Osaki. 2014. "Carbon Dioxide Emissions through Oxidative Peat Decomposition on a Burnt Tropical Peatland." *Global Change Biology* 20 (2): 555–565. doi:10.1111/gcb.2014.20.issue-2.

Huang, X., J. Wang, and J. Shang. 2016. "An Adaptive Two-Component Model- Based Decomposition on Soil Moisture Estimation for C-Band Radarsat-2 Imagery over Wheat Fields at Early Growing Stages." *IEEE Geoscience and Remote Sensing Letters* 13 (3): 414–418.

Iodice, A., A. Natale, and D. Riccio. 2011. "Retrieval of Soil Surface Parameters via a Polarimetric Two-Scale Model." *IEEE Transactions on Geoscience and Remote Sensing* 49 (7): 2531–2547. doi:10.1109/TGRS.2011.2106792.

Iodice, A., A. Natale, and D. Riccio. 2013. "Polarimetric Two-Scale Model for Soil Moisture Retrieval via Dual-Pol HH-VV SAR Data." *IEEE Journal of Selected Topics in Applied Earth Observations and Remote Sensing* 6 (3): 1163–1171. doi:10.1109/JSTARS.2013.2238893.

Ishii, Y., K. Koizumi, H. Fukami, K. Yamamoto, H. Takahashi, S. H. Limin, K. Kusin, A. Usup, and G. E. Susilo. 2016. "Groundwater in Peatland, edited by Mitsuru Osaki and Nobuyuki Tsuji." In *Tropical Peatland Ecosystems*, 265–279. Tokyo: Springer.

Jagdhuber, T. 2012. "Soil parameter retrieval under vegetation cover using SAR polarimetry." PhD diss., ETH Zurich. doi:10.1094/PDIS-11-11-0999-PDN

Jagdhuber, T., I. Hajnsek, K. P. Papathanassiou, and A. Bronstert. 2011. "A Hybrid Decomposition for Soil Moisture Estimation under Vegetation Cover Using Polarimetric SAR." In *Proceedings of ESA POLinSAR Workshop*, 1–6, Frascati, Italy.

Jaya, A., T. Hidenori, M. Takada, Y. Mishima, and I. Takashi. 2011. "Moisture Behavior of Surface Peat Layer in Areas of Different Surface Cover and Different Ground Condition during Dry Season in Central Kalimantan (PART 2)." In *Proceedings of international workshop on wild fire and carbon management in peat-forest in Indonesia 2011*, 197–202, Palangka Raya, Indonesia. doi:10.1094/PDIS-11-11-0999-PDN

Kausarian, H., J. T. S. Sumantyo, H. Kuze, J. Aminuddin, and M. M. Waqar. 2017. "Analysis of Polarimetric Decomposition, Backscattering Coefficient, and Sample Properties for Identification and Layer Thickness Estimation of Silica Sand Distribution Using L-Band Synthetic Aperture Radar." *Canadian Journal of Remote Sensing* 43 (2): 95–108. doi:10.1080/07038992.2017.1286935.

Koyama, C. N., H. Liu, K. Takahashi, M. Shimada, M. Watanabe, T. Khuut, and M. Sato. 2017. "In-Situ Measurement of Soil Permittivity at Various Depths for the Calibration and Validation of Low-Frequency SAR Soil Moisture Models by Using GPR." *Remote Sensing* 9 (6): 580. doi:10.3390/rs9060580.

Lee, J.-S., M. R. Grunes, and D. G. Gianfranco. 1999. "Polarimetric SAR Speckle Filtering and Its Implication for Classification." *IEEE Transactions on Geoscience and Remote Sensing* 37 (5): 2363–2373. doi:10.1109/36.789635.

Martino, D., A. I. Gerardo, A. Natale, and D. Riccio. 2016. "Polarimetric Two-Scale Two-Component Model for the Retrieval of Soil Moisture under Moderate Vegetation via L-Band SAR Data." *IEEE Transactions on Geoscience and Remote Sensing* 54 (4): 2470–2491. doi:10.1109/TGRS.2015.2502425.

Oh, Y. 2004. "Quantitative Retrieval of Soil Moisture Content and Surface Roughness from Multipolarized Radar Observations of Bare Soil Surfaces." *IEEE Transactions on Geoscience and Remote Sensing* 42 (3): 596–601. doi:10.1109/TGRS.2003.821065.

Osaki, Mitsuru, Dedi Nursyamsi, Muhammad Noor, Hendrik Segah. 2016. "Peatland in Indonesia, edited by Mitsuru Osaki and Nobuyuki Tsuji." In *Tropical Peatland Ecosystems*, 49–58. Tokyo: Springer.

Page, S. E., J. O. Rieley, and C. J. Banks. 2011. "Global and Regional Importance of the Tropical Peatland Carbon Pool." *Global Change Biology* 17 (2): 798–818. doi:10.1111/j.1365-2486.2010.02279.x.

Sundari, S., T. Hirano, H. Yamada, K. Kusin, and S. Limin. 2012. "Effect of Groundwater Level on Soil Respiration in Tropical Peat Swamp Forests." *Journal of Agricultural Meteorology* 68 (2): 121–134. doi:10.2480/agrmet.68.2.6.

Takahashi, H., A. Usup, H. Hayasaka, M. Kamiya, and S. H. Limin. 2004. "The Importance of Ground Water Level and Soil Moisture of Subsurface Layer on Peat/Forest Fire in a Tropical Peat Swamp Forest." In *Wise Use of Peatlands*. Paper presented at the annual meeting for the Society of Wise use of peatlands: Proceedings of the 12th International Peat Congress, Tampere, Finland, Juhani Päivänen, 760.

Topp, G. C., J. L. Davis, and A. P. Annan. 1980. "Electromagnetic Determination of Soil Water Content: Measurements in Coaxial Transmission Lines." *Water Resources Research* 16 (3): 574–582. doi:10.1029/WR016i003p00574.

Ulaby, F. T., F. Kouyate, A. K. Fung, and A. J. Sieber. 1982. "A Backscatter Model for a Randomly Perturbed Periodic Surface." *IEEE Transactions on Geoscience and Remote Sensing* 4: 518–528. doi:10.1109/TGRS.1982.350420.

Usup, A., Y. Hashimoto, H. Takahashi, and H. Hayasaka. 2004. "Combustion and Thermal Characteristics of Peat Fire in Tropical Peatland in Central Kalimantan, Indonesia." *Tropics* 14 (1): 1–19. doi:10.3759/tropics.14.1.

van Zyl, J. J., M. Arii, and Y. Kim. 2011. "Model-Based Decomposition of Polarimetric SAR Covariance Matrices Constrained for Nonnegative Eigenvalues." *IEEE Transactions on Geoscience and Remote Sensing* 49 (9): 3452–3459. doi:10.1109/TGRS.2011.2128325.

Yamaguchi, Y., T. Moriyama, M. Ishido, and H. Yamada. 2005. "Fourcomponent Scattering Model for Polarimetric SAR Image Decomposition." *IEEE Transactions on Geoscience and Remote Sensing* 43 (8): 1699–1706. doi:10.1109/TGRS.2005.852084.

Zribi, M., and M. Dechambre. 2003. "A New Empirical Model to Retrieve Soil Moisture and Roughness from C-Band Radar Data." *Remote Sensing of Environment* 84 (1): 42–52. doi:10.1016/S0034-4257(02)00069-X.